Polish Journal of Microbiology
2019, Vol. 68, No 4, 549–558
https://doi.org/10.33073/pjm-2019-057

ORIGINAL PAPER

Structural Changes of *Bacillus subtilis* Biomass on Biosorption of Iron (II) from Aqueous Solutions: Isotherm and Kinetic Studies

SRI LAKSHMI RAMYA KRISHNA KANAMARLAPUDI and SUDHAMANI MUDDADA*

Department of Biotechnology, Koneru Lakshmaiah Education Foundation (KLEF), Greenfields, Vaddeswaram, Guntur, Andhra Pradesh, India

Submitted 9 June 2019, revised 9 November 2019, accepted 11 November 2019

Abstract

Various microbial biomasses have been employed as biosorbents. Bacterial biomass has added advantages because of easy in production at a low cost. The study investigated the biosorption of iron from aqueous solutions by *Bacillus subtilis*. An optimum biosorption capacity of 7.25 mg of the metal per gram of the biosorbent was obtained by the Inductive Coupled Plasma Optical Emission Spectroscopy (ICP-OES) under the experimental conditions of initial metal concentration of 100 mg/l, pH 4.5, and biomass dose of 1 g/l at 30°C for 24 hrs. The data showed the best fit with the Freundlich isotherm model while following pseudo-first-order kinetics. Scanning Electron Microscope (SEM) and Energy Dispersive X-ray (EDX) analysis confirmed iron biosorption as precipitates on the bacterial surface, and as a peak in the EDX spectrum. The functional hydroxyl, carboxyl, and amino groups that are involved in biosorption were revealed by the Fourier Transform Infrared spectroscopy (FTIR). The amorphous nature of the biosorbent for biosorption was indicated by the X-ray Diffraction (XRD) analysis. The biomass of *B. subtilis* exhibited a point zero charge (pH_{pzc}) at 2.0.

Key words: *Bacillus subtilis*, biosorption, iron, isotherms, kinetics

Introduction

Remediation of metal ions from contaminated sites is paramount. Many industries and various human activities discharge large amounts of metal ions into the water bodies where they cannot be degraded or destroyed. Ultimately, heavy metal ions reach and accumulate in the tissues of animals and humans (Iheanacho et al. 2017) posing serious health ailments.

Some metal ions act as essential micronutrients for most of the living organisms as metalloenzymes when present in sufficient quantities. However, they become toxic at high concentrations (Bhattacharya et al. 2016). Hence, metal ion concentration in wastewater and drinking water sources has to be reduced to a set levels (0.1 mg/l – Fe; 1 mg/l – Cu; 5 mg/l – Zn; 0.05 mg/l – Ar; 0.005 mg/l – Cd; 0.001 mg/l – Hg; 0.05 mg/l – Pb; 0.01 mg/l – Se) as per standards set by WHO (Puri and Kumar 2012). The traditional chemical treatments used to remediate metal ions are connected with many drawbacks like high energy requirement, the formation of sludge or waste products, incomplete removal of ions, high cost and difficulty in implementation (Renu et al. 2017), and may become ineffective at low quantities (10–100 mg/l).

Biosorption has emerged as an alternative to traditional techniques. Biosorption is described as a naturally occurring metabolism that binds metal ions to the cellular structure of the biosorbents even from very dilute aqueous solutions (Shamim 2018). A microbial cell is a natural biosorbent of metal ions. Studies were done using microbial biomass (algae, bacteria, and fungi) as biosorbent for remediation of metal ions from polluted water resources. The biosorption process relies on nature and biosorbent type, and metal species to be biosorbed (El-Naggar et al. 2018).

The process of biosorption is associated with many advantages as a low operating cost, biosorbent reuse, the minimized disposal of chemical or biological sludge, detoxification of very dilute effluents with high efficiency, specific metal selectivity, low operation time, and no secondary toxic compounds production.

* Corresponding author: S. Muddada, Department of Biotechnology, Koneru Lakshmaiah Education Foundation (KLEF), Greenfields, Vaddeswaram, Guntur, Andhra Pradesh, India; **e-mail: sudhamani1@rediffmail.com**

Hence, the process of biosorption is promising for the remediation of heavy metals from polluted water bodies (Zawierucha et al. 2016).

Among trace elements, iron is required for most of the living organisms for the formation of hemoglobin. High iron levels (200–250 mg/kg body weight) in drinking water may cause many ill effects and can be lethal (Prashanth et al. 2015). The presence of a high level of iron in the food products also effects taste, color, and appearance due to reaction with the phenolic compounds (Dueik et al. 2017). Hence, it is necessary to remove iron ions.

Bacillus is a diverse group of microorganisms. Many species of *Bacillus* are found to have metal-binding properties (Wierzba 2015; Dey et al. 2016; García et al. 2016). *Bacillus subtilis* is non-pathogenic and non-toxic with a Generally Regarded as Safe (GRAS) status. The biosorption of metal ions by *B. subtilis* has been studied (Al-Gheethi et al. 2017; Cai et al. 2018). Besides, many studies reported the biosorption of iron by various microbial biosorbents (Keshtkar et al. 2016; Migahed et al. 2017). However, there is very little information regarding the structural and functional changes occurring on the biomass of *B. subtilis* as a consequence of iron biosorption.

Hence, in the present study iron removal was done by utilizing biomass of *B. subtilis* in aqueous solutions. Optimization of experimental parameters, isotherms, and kinetic studies was done to characterize iron biosorption onto the biomass. Also, changes on the surface of the biosorbent were evaluated.

Experimental

Materials and Methods

Microorganism and growth conditions. The strain, *Bacillus subtilis* (1427) was procured from Microbial Type Culture Collection (MTCC), Chandigarh. The stock culture of *B. subtilis* was preserved on nutrient agar plates at 4°C and subcultured every month. Bacterial stocks were maintained in 50% glycerol at –80°C. Fresh biomass was obtained by inoculating the strain in nutrient broth and incubating at 37°C for 24 hrs at 150 rpm. The bacterial culture obtained after centrifugation (8000 rpm, 10 min) was washed with distilled water and used as the biosorbent for iron biosorption experiments.

Preparation of metal solution. Stock solutions of $FeSO_4 \cdot 7H_2O$ (ferrous sulfate heptahydrate) were prepared in double-distilled water. Fresh working solutions were prepared before experiments.

Biosorption experiments. Biosorption of iron ions onto biomass of *B. subtilis* was done at 30°C by suspending different amounts of biosorbent in 100 ml metal ion solution in Erlenmeyer flasks (250 ml). The pH was adjusted by 1N NaOH or HCl before agitation at 100 rpm. The impact of various experimental parameters that influences the process of biosorption was examined. One target parameter was varied by keeping the others constant. Tests were performed with pH values varying from 3 to 9, initial metal ion concentrations differing from 4 to 40 mg/l, different inoculum sizes of 0.5 to 3 g/l, and different time intervals of 1–24 hrs. Controls (without the addition of metal) were maintained. After incubation, the biomass and supernatant obtained by centrifugation (8000 rpm, 10 min) were characterized separately.

Determination of residual Fe (II). Concentration of Fe (II) ions in the supernatant after biosorption experiments was obtained by the Inductive Coupled Plasma Optical Emission Spectroscopy (ICP-OES) at NCCCM, Hyderabad. At equilibrium conditions the percentage of biosorption and biosorption capacity of *B. subtilis* were obtained the equations:

$$qe = \frac{(Ci - Ce)\ V}{m}$$

$$R\% = \frac{(Ci - Ce)}{Ci} \times 100$$

where q_e is the quantity of the metal biosorbed by the biomass (mg/g) at equilibrium; C_i is initial metal (Fe) ion concentration in the solution (mg/l); C_e is the equilibrium metal (Fe) ion concentration in solution (mg/l), V is volume of the medium (l), and m is the quantity of the biomass used in the reaction mixture (g).

Isotherm modeling. In this study, the fit of experimental data was studied by the three most widely used models, namely Freundlich, Langmuir, and Temkin isotherms.

Linearized Langmuir isotherm model is shown as:

$$\frac{C_e}{q_e} = \frac{C_e}{q_m} + \frac{1}{K_L q_m}$$

where, q_e is the mass of metal ion biosorbed per gram of the biosorbent (mg/g); C_e is the final concentration of the metal ions (mg/l) in solution; q_m is the monolayer biosorption capacity of the biosorbent (mg/g), and k_L is the Langmuir biosorption constant (l/mg). The constants K_L and q_{max} were evaluated from the slope and the intercept of the linear plot of $1/q_e$ versus $1/C_e$

The affinity (R_L Hall isolation factor) of the biosorbent to the biosorbate can be calculated by the equation:

$$R_L = \frac{1}{1 + k_L C_i}$$

where C_i is the highest initial concentration of the biosorbate (mg/l).

Linearized Freundlich isotherm model is described as:

$$log\ q_e = log\ K_F + \frac{1}{n}\ log\ C_e$$

where, K_F is a constant for relative biosorption capacity of the biosorbent and 1/n is an experimental parameter of biosorption intensity, which can be calculated from the linear plot of log q_e versus log C_e.

Linearized Temkin isotherm model is shown as represented by the following equation:

$$q_e = \frac{RT}{b_T}\ lnA_T + \frac{RT}{b_T}\ lnC_e$$

where A_T is the Temkin isotherm equilibrium binding constant (L/g), b_T is the Temkin isotherm constant, R is universal gas constant (8.314 J/mol/K), and T is the temperature at 298 K. By plotting the values against q_e versus lnC_e the constants b_T and A_T can be determined.

Biosorption kinetics. In this study, pseudo-first-order and pseudo-second-order were applied.

Linear forms of the kinetic models are shown as:

$$\log\ (q_e - q_t) = log\ q_e - \frac{k_1 t}{2.303}$$

$$\frac{t}{q_t} = \frac{1}{k_2 \cdot q_e^2} + \frac{t}{q_e}$$

where q_e and q_t are the mass of Fe (II) ions biosorbed at equilibrium and at time t (mg/l), k_1 is the pseudo-first-order equilibrium rate constant (min^{-1}), k_2 is the pseudo-second-order rate constant (g mg^{-1} min^{-1}), and t is the contact time (min). The parameters of the two models can be calculated from the slope and intercept of linear plots of t versus log ($q_e - q_t$), and t versus t/q_t, respectively.

Scanning Electron Microscopy (SEM) and Energy Dispersive X-ray spectrometry (EDX) analysis. Morphology and elemental composition of biosorbent before and after biosorption with Fe(II) ions were examined by the Field Emission Scanning Electron Microscope (FE-SEM) (CARL ZEISS SUPRA 55 GEMIN-German Technology Jena, Germany). Biomass samples were glutaraldehyde fixed, attached to 10 mm alumina-based mounts and sputtered with gold particles by using sputter coater (SC7620 'Mini' sputter coater) under vacuum. Then, the obtained specimens were observed under SEM for capturing of images. Elemental composition (EDX) was analyzed by the Energy Dispersive X-ray spectrometry (EDX) (OXFORD EDS system) at 16 KeV voltage.

Fourier Transform Infrared Spectroscopy (FTIR). The Infrared spectrum of biosorbent before and after biosorption was recorded by the FTIR spectrometer (Thermo Nicolet Avatar 370 FTIR, Madison, US) to identify the functional groups on the biosorbent surface participating in biosorption. The samples were dried and mixed with KBr (1:200) and pressed to obtain transparent discs. The discs were analyzed immediately in the range of 400–4000 cm^{-1}, with KBr as background.

X-ray diffraction (XRD) analysis. Powdered biosorbent, before and after Fe (II) biosorption were characterized by X-ray diffraction apparatus (Bruker D8-Advance XRD model). The intensities of diffracted X-rays were noted as a function of 2θ angle by using monochromatic Cu-Kα (1.5406 Å) target radiations. The patterns were recorded over the range of 3° to 80° with a scan rate of 10°/min, and a step size of 0.02°. The conditions used for operating were 40 kV and 35 mA of current.

Determination of point zero charges (pH_{pzc}). The point zero charges of biosorbent were obtained by the pH drift method. For this, different conical flasks with 50 ml of 0.01 M NaCl solution were taken and pH (initial) was adjusted within the range of 2–12 by using either 0.1 M HCl or NaOH. After adjusting the pH, 0.15 g of *B. subtilis* biomass was put into all flasks and agitated for 48 hrs at room temperature. After incubation, the flasks were withdrawn from the shaker and the final pH was taken. The pH_{pzc} can be calculated from the plot of pH_{final} vs. $pH_{initial.}$ The intersection point of the curve ($pH_{initial} = pH_{final}$) was considered as the point of zero charge.

Results and Discussion

The bacterium *B. subtilis* is recognized as a GRAS organism (Sewalt et al. 2016), and hence, it is considered as a safe biosorbent for its use in metal remediation from polluted aqueous solutions.

Biosorption studies. The effect of different experimental parameters at various conditions was studied as discussed below.

Effect of initial metal ion concentration. The concentration of metal ion strongly influences the biosorbent biosorption capacity. From Fig. 1, it can be concluded that with the increase of metal ion concentration from 4 mg/l to 20 mg/l, the biosorption capacity

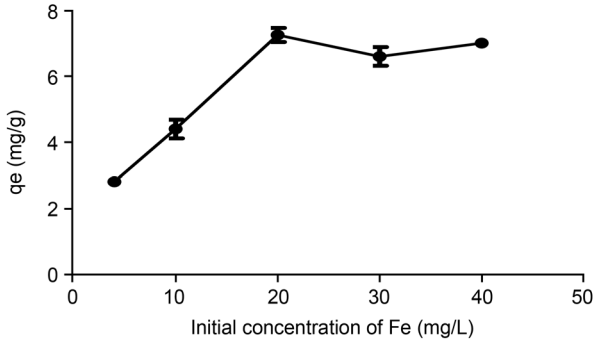

Fig. 1. Effect of initial concentration on biosorption of Fe (II) by *Bacillus subtilis* at a biomass concentration of 1 g/l, pH 4.5, and 100 rpm.

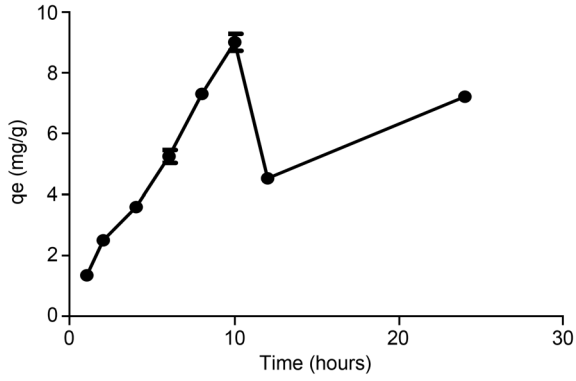

Fig. 2. Effect of contact time on biosorption Fe (II) by *Bacillus subtilis* at a biomass concentration of 1 g/l, pH 4.5, 20 mg/l of Fe (II) and 100 rpm.

Fig. 3. Effect of biosorbent dose on biosorption Fe (II) by *Bacillus subtilis* at initial metal ion concentration of 20 mg/l, pH 4.5, and 100 rpm.

increases from 2.8 mg per gram to 7.25 mg Fe(II) per gram of biosorbent, and thereafter, it remains almost constant with further increase of metal concentration (up to 40 mg/l). This phenomenon is due to that at low metal concentration the active sites present on the biosorbent are unoccupied leading to higher biosorption capacity. Due to the attainment of saturation with increasing metal concentration, further increase leads to lower or constant biosorption capacity. Hence, 20 mg/l metal concentration was taken as the optimum with the highest biosorption capacity of 7.25 mg of Fe (II)/g of the biomass. Similarly, in other studies with As (V) concentration ranging from 500–3000 µg/l, there was an increase in biosorption capacity and it reached equilibrium at the high metal concentration (Banerjee et al. 2016).

Effect of contact time. The biosorption capacity was increased from 1.35 to 9 mg/g of biomass with the increase in contact time up to 10 hrs due to the biosorption of metal ions with the available binding sites (Fig. 2). Upon further incubation, due to lowered availability of binding sites, and as repulsive forces existed between the bound Fe (II) ions and in those in solution, another stage of biosorption was noticed. A similar pattern of two-phase biosorption was observed for Cr (VI) ions with an increase in contact time from 10 min to 10 hrs (Arbanah et al. 2012).

Effect of the biosorbent dose. Different biomass dosages were considered as represented in Fig. 3. It shows that there was a decrease in biosorption capacity with the raise of biomass dosage from 0.5 g/l to 3 g/l. At higher dosage, the biomass forms aggregates that lead to a reduction in available binding sites resulting in lower biosorption capacity. Hence, the concentration of 1 g/l of biosorbent was taken as an optimum dose for biosorption of Fe (II) ions. These results are in line with other reported studies, where, with the increase of biosorbent dose of *Bacillus cereus* from 0.5 to 3 g/l, there was the decrease in biosorption capacity from 36.21 to 7.73 mg/g of biomass for Pb (II) ions (Todorova et al. 2019).

Effect of pH. One of the crucial parameters to be monitored during biosorption is pH because it influences the functional groups and heavy metal solution chemistry. At low pH, binding of metal ions to the biosorbent is reduced due to the existence of metal – proton competition to the same binding region (Farnane et al. 2018). However, in our experiments at a low pH of 3, the damage to the biomass occurred and resulted in the formation of flakes. At high pH values (pH > 4.5) precipitation of iron (results in yellowing of solution) and formation of hydroxides ($Fe(OH_3)^-$ and $Fe(OH_4)^{2-}$) occurred which hindered the biosorption. Hence, pH 4.5 was taken as an optimum in our studies to attain the highest biosorption capacity assuming that the functional groups are deprotonated and attained a negative charge for binding of positive metal ions. Also, many studies reported that biosorption is meaningless at higher pH due to the occurrence of metal hydroxides causing difficulty in concluding whether the decrease in metal concentration was due to lowered biosorption or precipitation (El-Naggar et al. 2018).

Isotherm modeling. The metal ion biosorption capacity of biosorbent was determined by the equilibrium sorption isotherms that characterize the affinity and surface properties of the biosorbent by expressing certain constant values (Kariuki et al. 2017). The present study used three biosorption isotherm models, namely Langmuir, Freundlich, and Temkin isotherms.

Langmuir isotherm can be described as a quantitative monolayer occurrence of the biosorbate on the biosorbent surface, containing the unbounded number of active sites (Saraf and Vaidya 2016). The Freundlich isotherm model explains heterogeneous surface biosorption where enthalpy of biosorption is independent of the metal ion biosorbed (Ahad et al. 2017). Temkin isotherm is showed by considering the factor of biosorbate – biosorbent interaction explicitly into

Table I
Constants of Langmuir, Freundlich and Temkin isotherm models used for the biosorption of Fe (II) ions onto *B. subtilis* biomass.

Langmuir isotherm		Freundlich isotherm		Temkin isotherm	
q_{max} (mg/g)	3.831	n	3.425	B (J/mol)	1.3583
K_L (l/mg)	1.845	K_F (mg/g)	2.766	A (l/g)	6.78 g/l
R^2	0.9353	R^2	0.9057	R^2	0.8715
R_L	0.013				

account and presume that there was a linear decrease in biosorption heat of solute molecules in the layer rather than logarithmically (Ahad et al. 2017).

From the respective linear plots, the constants of three isotherms models obtained are presented in Table I. Based on the regression coefficient value (R^2), the biosorption data expressed shows best fit with Langmuir isotherm model (0.9353) compared to Freundlich (0.9057), and Temkin isotherm models (0.8715) indicating that Fe (II) biosorption onto *B. subtilis* is monolayer with uniform binding energy. The value of $R_L = 0$ indicates favorable biosorption. The value of 'n' is greater than unity suggesting that the iron ions are favorably biosorbed onto *B. subtilis* biomass. The constants of Temkin isotherm suggest that the heat of sorption is a physical process. Various studies reported that either Freundlich (Safari and Ahmady-Asbchin 2018), Langmuir (Anuradha et al. 2018) or Temkin (Aravind et al. 2015) isotherm models are the best fit.

Biosorption kinetics. The kinetics expresses the rate of biosorption by determining the residence time of biosorbate for the completion of biosorption at the solid-solution interface. It also determines the mode of biosorption and the possible rate-controlling steps either in mass transport (pseudo-first-order) or in chemical reaction (pseudo-second-order). The kinetics of Fe (II) biosorption onto *B. subtilis* can be evaluated by subjecting the experimental data to two kinetic models – pseudo-first and second-order models.

From the respective linear plots, the parameters of two kinetic models were obtained which were summarized in Table II. With a high correlation coefficient (R^2) and the low difference between the experimental and calculated q_e values, we can interpret that the data fits well with pseudo-first-order kinetic model. The rate-controlling step is diffusion and does not depend on the concentration of both the reactants which implies that the biosorption is physisorption. Other studies also reported that pseudo-first-order kinetic model as a better fit for biosorption of Pb (II) and Zn (II) ions. (Hanbali et al. 2014; Singh and Chopra 2014).

SEM-EDX analysis. Morphological changes that occurred as a result of Fe (II) biosorption onto *B. subtilis* were visualized by scanning electron microscopy (SEM). SEM images revealed that before biosorption the cells were found to be plump with smooth surfaces in loosely bound form. After biosorption with Fe (II) ions, cells showed the presence of bulky particles in the form of precipitates on the surface, increase in cell size and roughness of the cell (Fig. 4 and 5). Similarly, the alteration in morphology of *Ralstonia pickettii* and lactic acid bacteria biomass was observed due to biosorption of Mn (II) and Fe (II), respectively (Ramyakrishna and Sudhamani 2017; Huang et al. 2018).

The Energy Dispersive Spectroscopy (EDX) analysis is used to indicate the presence of metal. The peak for iron in the spectrum confirmed that the Fe (II) ions were biosorbed onto the *B. subtilis* biomass (Fig. 5). The composition of elements in the biomass loaded with Fe (II) differed from that of the control biomass. The elements Magnesium, Sodium, and Calcium which were initially present in the control (Fig. 4) were not observed in the metal-loaded biomass, which indicated that iron replaced the other metal ions that already existed on the biosorbent surface. Further, the percentage composition of Oxygen, Phosphorus and Potassium in the metal loaded biomass was lowered which indicates that the mechanism of ion exchange plays a role in biosorption of Fe (II) ions. A similar mechanism of ion exchange was observed in other studies for Fe (II) biosorption by lactic acid bacteria (Ramyakrishna and Sudhamani 2017).

Table II
Constants of pseudo-first and pseudo-second-order kinetic models obtained for the biosorption of Fe (II) ions onto *B. subtilis*.

Pseudo-first-order kinetic model			Pseudo-second-order kinetic model		
q_e (mg/g),	K_1 (min^{-1})	R^2	q_e (mg/g)	K_2 ($gmg^{-1}\ min^{-1}$)	R^2
10.6	0.2001	0.9201	17.76	0.0042	0.7154

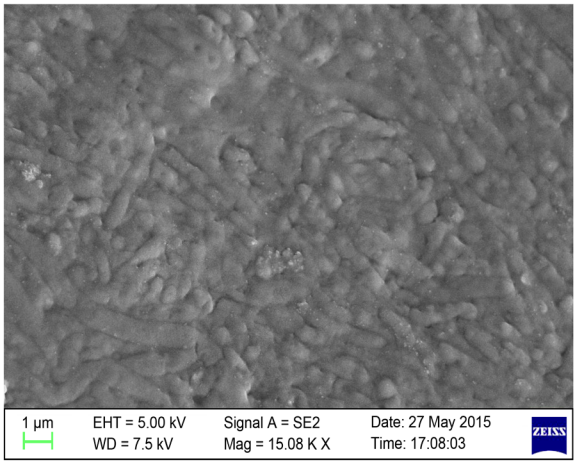

Element	Weight %	Atomic %	Element	Weight %	Atomic %
C	66.27	73.55	P	2.33	1.00
O	29.51	24.59	S	0.37	0.15
Na	0.39	0.22	Cl	0.15	0.06
Mg	0.32	0.17	K	0.27	0.09
Si	0.17	0.08	Ca	0.22	0.07

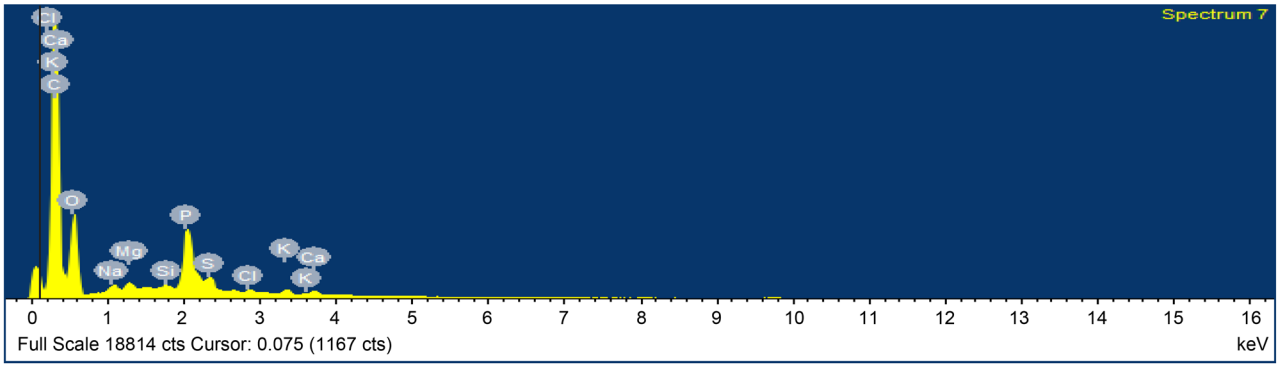

Fig. 4. SEM image, EDX spectra and elemental composition of unloaded (control) biomass of *B. subtilis*.

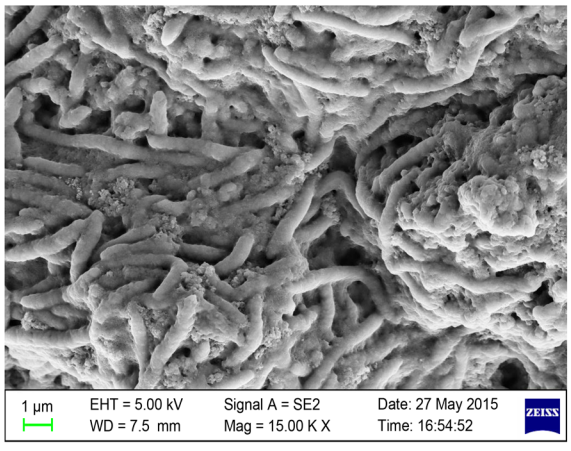

Element	Weight %	Atomic %	Element	Weight %	Atomic %
C	70.37	77.68	S	0.48	0.20
O	25.01	20.73	Cl	0.14	0.05
Si	0.37	0.18	K	0.08	0.03
P	1.58	0.68	Fe	1.96	0.47

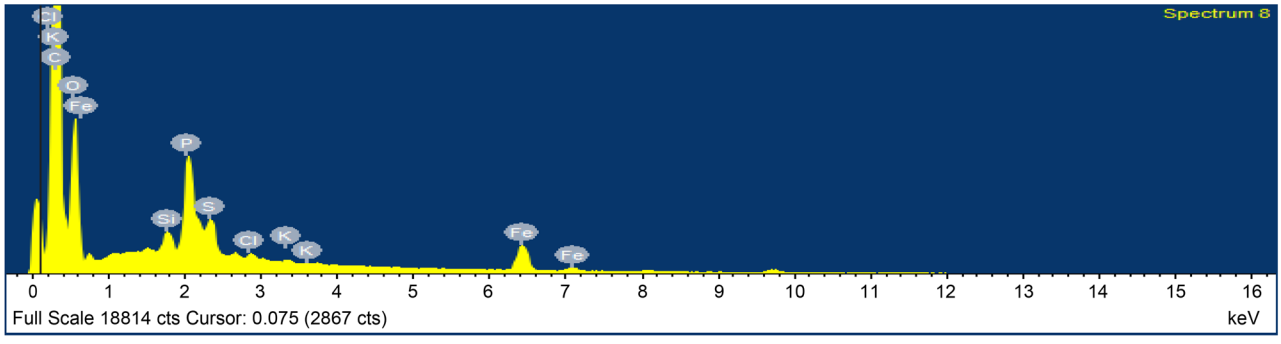

Fig. 5. SEM image, EDX spectra and elemental composition of *B. subtilis* biosorbed with Fe (II) ions.

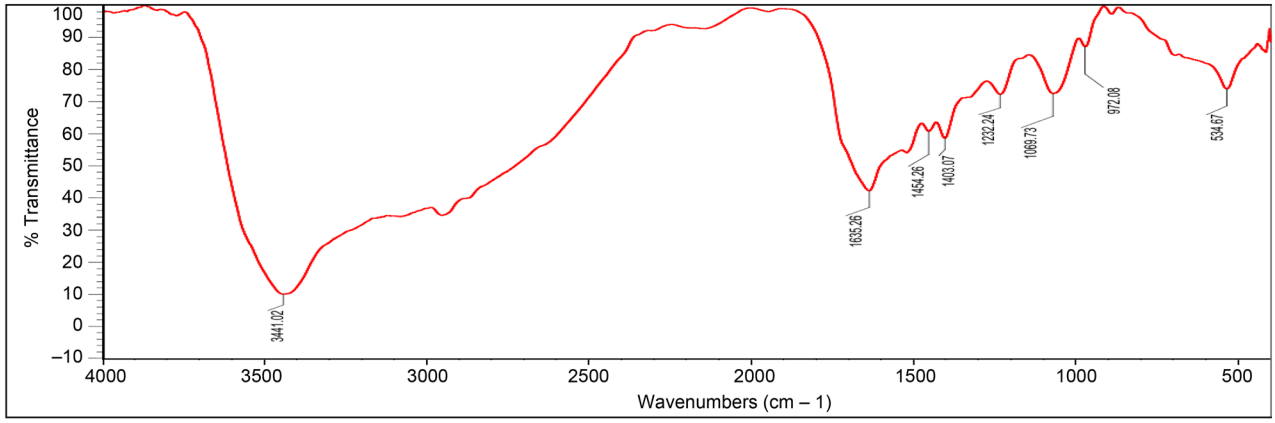

Fig. 6a. FTIR spectra of unloaded (control) biomass of *B. subtilis*.

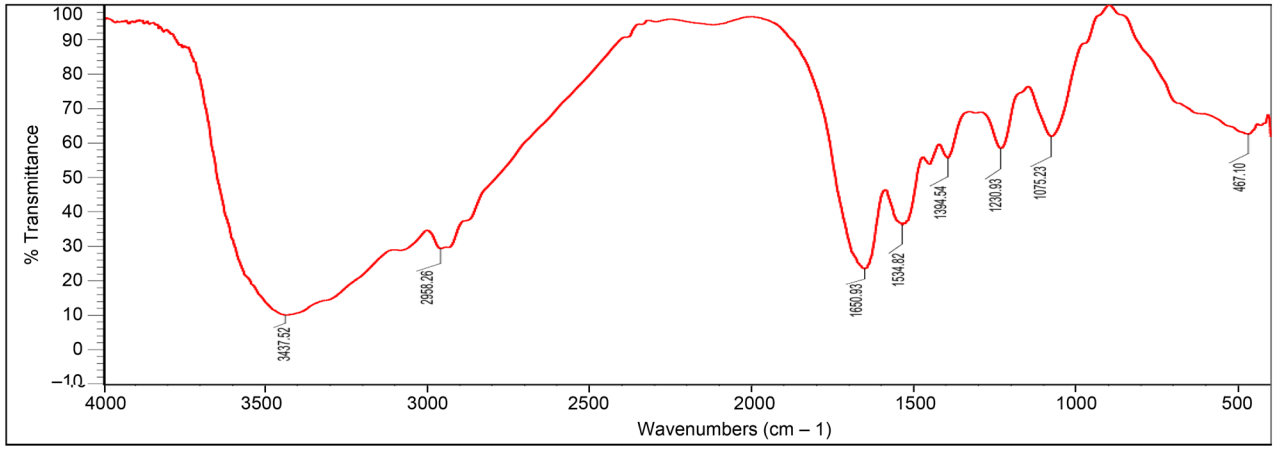

Fig. 6b. FTIR spectra of Fe (II) ion biosorbed by *B. subtilis* biomass.

FTIR analysis. FTIR spectrum discloses the functional groups that take part in Fe (II) biosorption. The spectrum of the biosorbent displayed varied biosorption peaks indicating the composite nature of the biomass. Figure 6a shows the IR spectrum of control biomass. The broad peak at 3441 cm^{-1} indicates the presence of –OH and –NH stretching, thus televising the occurrence of hydroxyl and amine groups. The peak at 1635 cm^{-1} represents the appearance of the amide group. Peaks at 1454 cm^{-1} and 1403 cm^{-1} shows the stretching of –C–C=C groups and C–H bending of the aromatic ring, respectively. The –C–O stretching of the carboxyl group was displayed at 1232 cm^{-1}. The peaks at 1069 cm^{-1} and 972 cm^{-1} represent the –C–C stretching of alcohols and C–O–C, C–O, C–O–P bonds of polysaccharides.

The IR spectrum of metal loaded biomass (Fig. 6b) showed significant changes in the range of 3437 cm^{-1}, 1650 cm^{-1}, 1230 cm^{-1}, and at 1075 cm^{-1} indicating that these functional groups participate in metal ion biosorption. A new peak formed at 2958 cm^{-1} indicated the stretching of –C–H bond of the aliphatic methylene group. Stretching of COO^- bond of carboxylate group appeared at 1534 cm^{-1}. The peak at 1394 cm^{-1} indicates the C=C stretching vibration of alkyl side chains. The bands below 800 cm^{-1} indicate the fingerprint zone, which can be attributed to phosphate and sulfur functional groups. Additionally, a clear shift in the protein region (3437 cm^{-1}, 1650 cm^{-1}) is exhibited indicating the protein role in Fe (II) biosorption. Conclusively, changes in the frequencies of these functional groups indicate that they participate in biosorption process. Similar changes in the FTIR spectrum due to arsenic biosorption were reported by Cristobel (Christobel and Lipton 2015). Changes at 3411 cm^{-1}, 2929 cm^{-1}, 1239 cm^{-1}, 1052 cm^{-1}, and 617 cm^{-1} peak intensities are in line with other reports (Dhanwal et al. 2018).

XRD analysis. The patterns of X-ray diffraction of *B. subtilis* prior and following iron biosorption are explained in Fig. 7a and 7b. Sharp intensity peak in the unloaded biosorbent has been observed at $2\theta = 16.610$ with d spacing value of 5.3392, whereas the pattern in the iron-bound biosorbent showed the emergence of new peaks at 2θ values of around 8.293 and 19.659 indicating the crystalline character of the biosorbent.

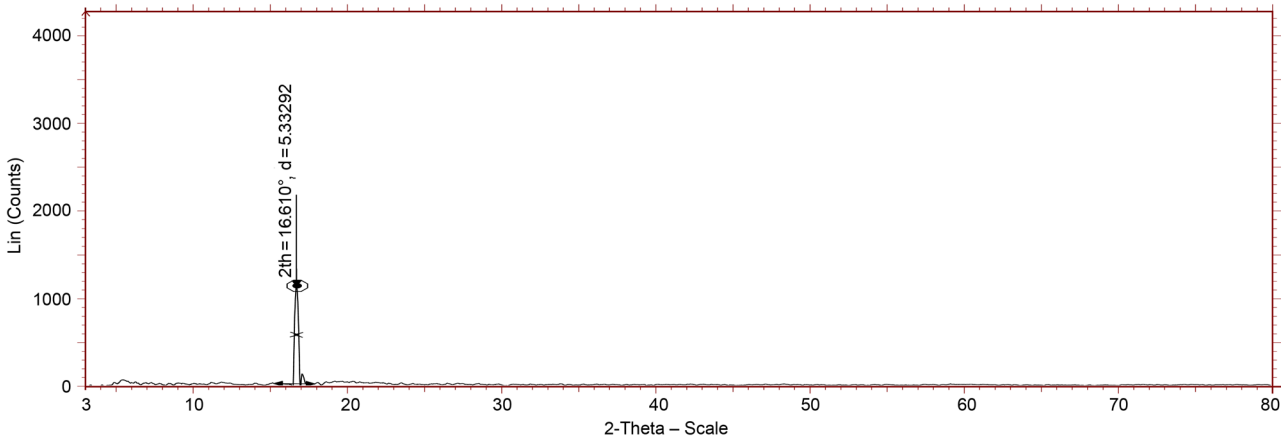

Fig. 7a. X-ray diffraction pattern of *B. subtilis* before biosorption with Fe (II) ions.

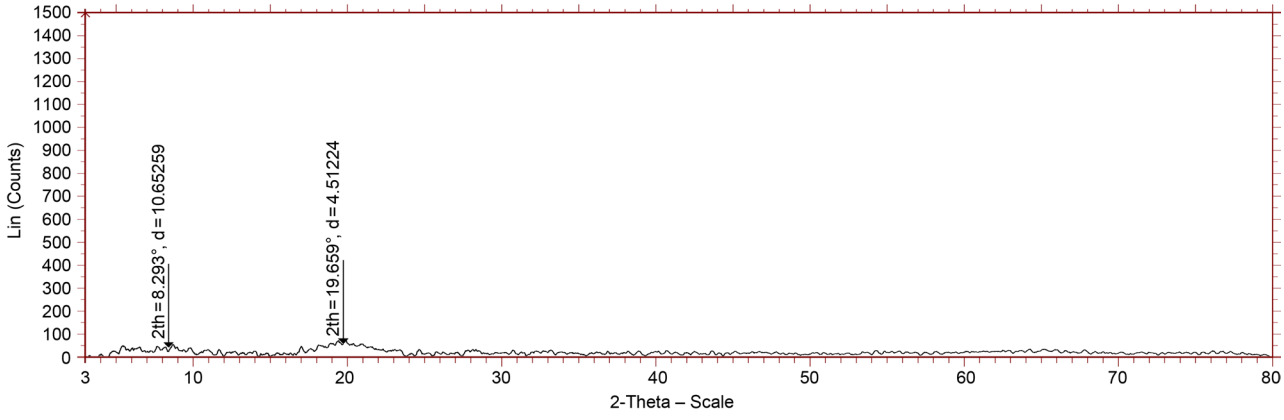

Fig. 7b. X-ray diffraction pattern of *B. subtilis* after biosorption with Fe (II) ions.

The amorphous character of biosorbent in the spectra is indicated by the poorly resolved peaks, which suggest that the metal ion can simply pierce into the surface; which is advantageous for metal biosorption from aqueous solutions. The results are in agreement with other studies (Qu et al. 2015; Santuraki and Muazu 2015).

Point zero charge of biosorbent (pH_{pzc}). Metal biosorption onto biosorbent surface is based on pH, since it influences surface available binding sites of biosorbent and metal ions in solution, respectively. Hence, the calculation of point zero charges is a critical parameter to predict metal ion biosorption. As shown in Fig. 8, the pH_{pzc} of *B. subtilis* was found to be 2 indicating the positive charge of biosorbent at pH less than 2 and a negative charge at pH greater than 2. At pH < 2, metal proton competition exists resulting in the decline of biosorption. On the other hand, at pH > 2, the biosorbent is negatively charged which facilitates the electrostatic attraction with the positively charged metal ions resulting in maximum biosorption. At higher pH (pH < 6), a reduction in biosorption was also observed. This is because, at high pH values, there is a probability for precipitation of metal ions as salts or hydroxides in solution (Zaib et al. 2016). Similar results were observed using other strains of *B. subtils,* where the pH_{pzc} of the biosorbent was 1.5 (Ng 2018).

Conclusion

Analysis by ICP-OES and SEM-EDX showed that metal ions were biosorbed onto the biosorbent. Freundlich adsorption isotherm and pseudo-first-order kinetic model proved the better fit for experimental

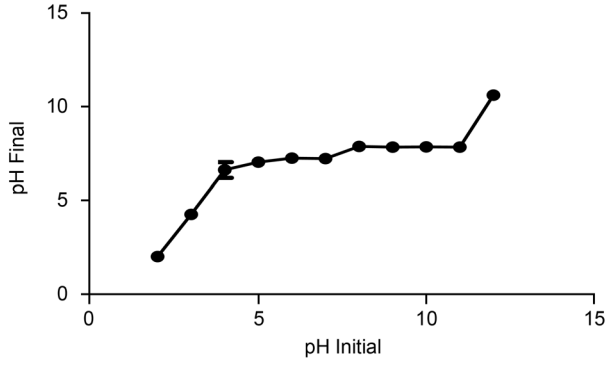

Fig. 8. Point zero charge (pHpzc) of *B. subtilis.*

data. The FTIR spectrum identified the possible functional groups that interact in metal biosorption. The amorphous nature of the biosorbent which is suitable for biosorption was revealed by XRD analysis. Point zero charge of biosorbent shows that the biosorption process is facilitated at pH > 2. At optimized experimental conditions of 100 mg/l of the metal ion at pH 4.5, with 1 g/l of biosorbent at 30°C for 24 hrs, the biomass of *B. subtilis* showed biosorption capacity of 7.25 mg of Fe (II)/g of biomass. The biomass of *B. subtilis* can be employed as a promising biosorbent for remediation of metal ions from polluted water sources.

Acknowledgments

The authors thank Mr. Arul Maximus Rabel, Center for Nano science and Nanotechnology, Satyabhama University, Chennai for the support on SEM–EDX analysis. The authors acknowledge Sophisticated Test and Instrumentation Center (SAIF), Kochi for FTIR and XRD analysis. Additionally, the authors thank NCCCM (BARC), Hyderabad for ICP-OES analysis.

Conflict of interest

The authors do not report any financial or personal connections with other persons or organizations, which might negatively affect the contents of this publication and/or claim authorship rights to this publication.

The work was partially funded under "SEED/WS/052/2015".

Literature

Ahad RIA, Goswami S, Syiem MB. Biosorption and equilibrium isotherms study of cadmium removal by *Nostoc muscorum* Meg 1: morphological, physiological and biochemical alterations. 3 Biotech. 2017;7(2):104.

Al-Gheethi A, Mohamed R, Noman E, Ismail N, Kadir OA. Removal of heavy metal ions from aqueous solutions using *Bacillus subtilis* biomass pre-treated by supercritical carbon dioxide. CLEAN-Soil, Air. Water. 2017;45(10):1700356.

Anuradha R Mulik, Preeti Kulkarni, Bhadekar RK. Biosorption studies on nickel and chromium by *Kocuria sp.* BRI 36 Biomass. Int J Appl Eng Res. 2018;13(9):6886–6893.

Aravind J, George LE, Kanmani P, Muthukumaran M. Biosorption of chromium using *A. towneri* and *R. eutropha*. Res Biotechnol. 2015;6(3):01–09.

Arbanah M, Najwa MM, Halim KK. Biosorption of Cr (III), Fe (II), Cu (II), Zn (II) ions from liquid laboratory chemical waste by *Pleurotus ostreatus.* Int J Biotechnol Wellness Ind. 2012; 1(3):152–162. doi:10.6000/1927-3037/2012.01.03.01

Banerjee A, Sarkar P, Banerjee S. Application of statistical design of experiments for optimization of As(V) biosorption by immobilized bacterial biomass. Ecol Eng. 2016 Jan;86:13–23. doi:10.1016/j.ecoleng.2015.10.015

Bhattacharya PT, Misra SR, Hussain M. Nutritional aspects of essential trace elements in oral health and disease: an extensive review. Scientifica (Cairo). 2016;2016:1–12. doi:10.1155/2016/5464373

Cai Y, Li X, Liu D, Xu C, Ai Y, Sun X, Zhang M, Gao Y, Zhang Y, Yang T, et al. A Novel Pb-resistant *Bacillus subtilis* bacterium isolate for co-biosorption of hazardous Sb (III) and Pb (II): thermodynamics and application strategy. Int J Environ Res Public Health. 2018 Apr 09;15(4):702. doi:10.3390/ijerph15040702

Christobel J, Lipton A. Evaluation of macroalgal biomass for removal of heavy metal arsenic (As) from aqueous solution. Int J Appl Innov Eng Manag. 2015;4(5):94–104.

Dey U, Chatterjee S, Mondal NK. Isolation and characterization of arsenic-resistant bacteria and possible application in bioremediation. Biotechnol Rep (Amst). 2016 Jun;10:1–7. doi:10.1016/j.btre.2016.02.002

Dhanwal P, Kumar A, Dudeja S, Badgujar H, Chauhan R, Kumar A, Dhull P, Chhokar V, Beniwal V. Biosorption of heavy metals from aqueous solution by bacteria isolated from contaminated soil. Water Environ Res. 2018 May 01;90(5):424–430. doi:10.2175/106143017X15131012152979

Dueik V, Chen BK, Diosady LL. Iron-polyphenol interaction reduces iron bioavailability in fortified tea: competing complexation to ensure iron bioavailability. J Food Qual. 2017;2017:1–7. doi:10.1155/2017/1805047

El-Naggar NEA, Hamouda RA, Mousa IE, Abdel-Hamid MS, Rabei NH. Biosorption optimization, characterization, immobilization and application of *Gelidium amansii* biomass for complete Pb^{2+} removal from aqueous solutions. Sci Rep. 2018 Dec;8(1):13456. doi:10.1038/s41598-018-31660-7

Farnane M, Machrouhi A, Elhalil A, Abdennouri M, Qourzal S, Tounsadi H, Barka N. New sustainable biosorbent based on recycled deoiled carob seeds: optimization of heavy metals remediation. J Chem. 2018 Oct 09;2018:1–16. doi:10.1155/2018/5748493

García R, Campos J, Cruz JA, Calderón ME, Raynal ME, Buitrón . Biosorption of Cd, Cr, Mn, and Pb from aqueous solutions by *Bacillus* sp. strains isolated from industrial waste activate sludge. TIP. 2016 Jan;19(1):5–14. doi:10.1016/j.recqb.2016.02.001

Hanbali M, Holail H, Hammud H. Remediation of lead by pretreated red algae: adsorption isotherm, kinetic, column modeling and simulation studies. Green Chem Lett Rev. 2014 Oct 02;7(4): 342–358. doi:10.1080/17518253.2014.955062

Huang H, Zhao Y, Xu Z, Ding Y, Zhang W, Wu L. Biosorption characteristics of a highly Mn(II)-resistant *Ralstonia pickettii* strain isolated from Mn ore. PLoS One. 2018 Aug 31;13(8):e0203285. doi:10.1371/journal.pone.0203285

Iheanacho EU, Ndulaka J, Onuh C. Environmental pollution and heavy metals. Environ Pollut. 2017;5(5):2321–9122.

Kariuki Z, Kiptoo J, Onyancha D. Biosorption studies of lead and copper using rogers mushroom biomass *'Lepiota hystrix'*. South Af J Chem Eng. 2017;23:62–70.

Keshtkar M, Dobaradaran S, Akbarzadeh S, Bahreini M, Abadi DRV, Nasab SG, Soleimani F, Khajeahmadi N, Baghmolaei M. Iron biosorption from aqueous solution by *Padina sanctae* crucis algae: isotherm, kinetic and modeling. Int J Pharm Technol. 2016; 1:10459–10471.

Puri A, Kumar M. A review of permissible limits of drinking water. Indian J Occup Environ Med. 2012;16(1):40–44. doi:10.4103/0019-5278.99696

Migahed F, Abdelrazak A, Fawzy G. Batch and continuous removal of heavy metals from industrial effluents using microbial consortia. Int J Environ Sci Technol. 2017 Jun;14(6):1169–1180. doi:10.1007/s13762-016-1229-3

Ng W. Surface charge characteristics of *Bacillus subtilis* NRS-762 cells. Peer J Preprints. 2018;6:e26626v1.

Prashanth L, Kattapagari KK, Chitturi RT, Baddam VRR, Prasad LK. A review on role of essential trace elements in health and disease. J Dr NTR Univ Health Sci. 2015;4(2):75–85. doi:10.4103/2277-8632.158577

Qu J, Zang T, Gu H, Li K, Hu Y, Ren G, Xu X, Jin Y. Biosorption of copper ions from aqueous solution by *Flammulina velutipes* spent substrate. BioResources. 2015 Oct 16;10(4):8058–8075. doi:10.15376/biores.10.4.8058-8075

Ramyakrishna K, Sudhamani M. The metal binding potential of a dairy isolate. J Water Reuse Desalin. 2017 Dec;7(4):429–441. doi:10.2166/wrd.2016.127

Renu NA, Agarwal M, Singh K. Methodologies for removal of heavy metal ions from wastewater: an overview. Interdiscip Environ Rev. 2017;18(2):124–142. doi:10.1504/IER.2017.087915

Safari M, Ahmady-Asbchin S. Biosorption of zinc from aqueous solution by cyanobacterium *Fischerella ambigua* ISC67: optimization, kinetic, isotherm and thermodynamic studies. Water Sci Technol. 2018 Oct 15;78(7):1525–1534. doi:10.2166/wst.2018.437

Santuraki AH, Muazu AA. Accessing the potential of *Lonchocarpus laxiflorus* roots (LLR) plant biomass to remove Cadmium (II) ions from aqueous solutions: equilibrium and kinetic studies. Afr J Pure Appl Chem. 2015 May 31;9(5):105–112. doi:10.5897/AJPAC2015.0620

Saraf S, Vaidya VK. Elucidation of sorption mechanism of *R. arrhizus* for reactive blue 222 using equilibrium and kinetic studies. J Microb Biochem Technol. 2016;8(3):236–246. doi:10.4172/1948-5948.1000292

Sewalt V, Shanahan D, Gregg L, La Marta J, Carrillo R. The Generally Recognized as Safe (GRAS) process for industrial microbial enzymes. Ind Biotechnol (New Rochelle NY). 2016 Oct; 12(5):295–302. doi:10.1089/ind.2016.0011

Shamim S. Biosorption of heavy metals. In: Derco J, Vrana B, editors. Biosorption. London (UK): IntechOpen Ltd.; 2018. p. 21–49.

Singh PP, Chopra AK. Removal of Zn2+ and Pb2+ using new isolates of *Bacillus* spp. PPS03 and *Bacillus subtilis* PPS04 from paper mill effluents using indigenously designed Bench-top Bioreactor. J Appl Nat Sci. 2014 Jun 01;6(1):47–56. doi:10.31018/jans.v6i1.374

Todorova K, Velkova Z, Stoytcheva M, Kirova G, Kostadinova S, Gochev V. Novel composite biosorbent from *Bacillus cereus* for heavy metals removal from aqueous solutions. Biotechnol Biotechnol Equip. 2019 Jan;33(1):730–738. doi:10.1080/13102818.2019.1610066

Wierzba S. Biosorption of lead(II), zinc(II) and nickel(II) from industrial wastewater by *Stenotrophomonas maltophilia* and *Bacillus subtilis*. Pol J Chem Technol. 2015 Mar 1;17(1):79–87. doi:10.1515/pjct-2015-0012

Zaib M, Athar MM, Saeed A, Farooq U, Salman M, Makshoof MN. Equilibrium, kinetic and thermodynamic biosorption studies of Hg(II) on red algal biomass of *Porphyridium cruentum*. Green Chem Lett Rev. 2016 Oct;9(4):179–189. doi:10.1080/17518253.2016.1185166

Zawierucha I, Kozlowski C, Malina G. Immobilized materials for removal of toxic metal ions from surface/groundwaters and aqueous waste streams. Environ Sci - Proc Imp. 2016;18(4):429–444.